Optical imaging of tissue mitochondrial redox state in intact rat lungs in two models of pulmonary oxidative stress

Reyhaneh Sepehr
Kevin Staniszewski
Sepideh Maleki
Elizabeth R. Jacobs
Said Audi
Mahsa Ranji

Optical imaging of tissue mitochondrial redox state in intact rat lungs in two models of pulmonary oxidative stress

Reyhaneh Sepehr,[a] Kevin Staniszewski,[a] Sepideh Maleki,[a] Elizabeth R. Jacobs,[b] Said Audi,[b,c] and Mahsa Ranji[a]
[a]University of Wisconsin Milwaukee, Biophotonics Lab, Department of Electrical Engineering, Milwaukee, Wisconsin 53211
[b]Pulmonary Division, Zablocki VA Medical Center, Milwaukee, Wisconsin 53295
[c]Marquette University, Department of Biomedical Engineering, Milwaukee, Wisconsin 53233

Abstract. Ventilation with enhanced fractions of O_2 (hyperoxia) is a common and necessary treatment for hypoxemia in patients with lung failure, but prolonged exposure to hyperoxia causes lung injury. Ischemia-reperfusion (IR) injury of lung tissue is common in lung transplant or crush injury to the chest. These conditions are associated with apoptosis and decreased survival of lung tissue. The objective of this work is to use cryoimaging to evaluate the effect of exposure to hyperoxia and IR injury on lung tissue mitochondrial redox state in rats. The autofluorescent mitochondrial metabolic coenzymes nicotinamide adenine dinucleotide (NADH) and flavin adenine dinucleotide (FAD) are electron carriers in ATP generation. These intrinsic fluorophores were imaged for rat lungs using low-temperature fluorescence imaging (cryoimaging). Perfused lungs from four groups of rats were studied: normoxia (control), control perfused with an mitochondrial complex IV inhibitor (potassium cyanide, KCN), rats exposed to hyperoxia (85% O_2) for seven days, and from rats subjected to lung IR *in vivo* 24 hours prior to study. Each lung was sectioned sequentially in the transverse direction, and the images were used to reconstruct a three-dimensional (3-D) rendering. In KCN perfused lungs the respiratory chain was more reduced, whereas hyperoxic and IR lung tissue have a more oxidized respiratory chain than control lung tissue, consistent with previously measured mitochondrial dysfunction in both hyperoxic and IR lungs. © *2012 Society of Photo-Optical Instrumentation Engineers (SPIE).* [DOI: 10.1117/1.JBO.17.4.046010]

Keywords: optical imaging; nicotinamide adenine dinucleotide; flavin adenine dinucleotide; mitochondrial redox; lung tissue; hyperoxia; ischemia-reperfusion.

Paper 11581 received Oct. 7, 2011; revised manuscript received Feb. 3, 2012; accepted for publication Feb. 14, 2012; published online Apr. 19, 2012.

1 Introduction

Fluorescence imaging techniques provide both anatomical and functional information of tissue via intrinsic fluorophores or exogenous tagged proteins.[1] These techniques are widely used to probe tissue redox state and energy homeostasis in organs such as the heart,[2] brain,[3] kidney,[4–6] liver,[7] skeletal muscle,[8] cervix,[9] and colon,[10] as well as to diagnose diseases, such as breast cancer tumor localization and oxygenation.[11,12] Furthermore, these techniques have been shown to have a high sensitivity and specificity for discriminating between diseased and nondiseased tissue.[13]

Tissue metabolic state, which is an indicator of cellular oxygen consumption, can be extracted from fluorescence images of intrinsic fluorophores.[14,15] The mitochondrial metabolic coenzymes nicotinamide adenine dinucleotide (NADH) and flavin adenine dinucleotide ($FADH_2$) are the primary electron carriers in oxidative phosphorylation. NADH and $FADH_2$ oxidation via the electron transport chain results in the translocation of protons from complexes I, III, and IV across the inner mitochondrial membrane into the mitochondrial inner membrane region. The resulting proton gradient across the inner mitochondrial membrane, along with adenosine diphosphate (ADP) availability, controls the rate of mitochondrial adenosine triphosphate (ATP) synthesis, which accounts for ~90% of ATP production in lung tissue. Thus, a change in redox ratio (RR) is an index of a change in lung tissue bioenergetics.[16]

NADH and FAD (oxidized form of $FADH_2$) are autofluorescent and can be monitored without exogenous labels by noninvasive optical techniques.[17] The fluorescence signals of these intrinsic fluorophores have been used as indicators of tissue metabolism in injuries due to hypoxia, ischemia, and cell death.[18] Ranji et al. demonstrated that the ratio of these fluorophores, termed the mitochondrial redox ratio (RR = NADH/FAD), is a marker of the mitochondrial redox and metabolic state of myocardial tissue in intact hearts or *in vivo* situations.[19–22] There is more than one definition for redox ratio, including the normalized redox ratio [NADH/(NADH + FAD)];[18] the definition that is used in this study (NADH/FAD) is chosen since the FAD signal in lung tissue, as compared to the NADH signal, is significantly smaller than in other organ tissues such as the heart. Thus, the normalized redox ratio would be less sensitive to a change in mitochondrial redox state than NADH/FAD.

Rapid freeze trapping of organs in liquid nitrogen temperatures preserves the tissue metabolic state. Subsequent low-temperature fluorescence imaging (cryoimaging) is advantageous since it provides high fluorescence quantum yield of NADH and FAD as compared with room temperature, and 3-D spatial distribution of tissue NADH and FAD fluorescence intensities.[21,23,24]

Address all correspondence to: Mahsa Ranji, University of Wisconsin Milwaukee, Biophotonics Lab, Department of Electrical Engineering, , Milwaukee, Wisconsin 53211. Tel: 414-229-6619; Fax: 414-229-6958; E-mail: ranji@uwm.edu

Exposure to elevated O_2 (hyperoxia) is a common and necessary therapy for adult and pediatric patients with acute respiratory distress syndrome to restore blood oxygen tension (PO_2) to a level that sustains vital organ metabolic requirements.[25,26] However, sustained exposure to high O_2 (>50%) causes lung O_2 toxicity injury. This injury, which is the result of enhanced production of reactive O_2 species (ROS), i.e., oxidative stress, may further impair lung function and contribute to the very dysfunction that it is intended to alleviate.[27,28]

Ischemia-reperfusion (IR) injury of lung tissues is commonly encountered clinically in conditions such as lung transplantation, necrotizing pneumonias, or crush injury to the chest.[29] Approximately 1500 lung transplants are performed each year in the U.S.,[30] with many times that number lost due to prohibitive ischemic times. In both the above circumstances, the capacity to distinguish the oxidative state of individual lungs would modify management.

Mitochondrial dysfunction is a cardinal feature of hyperoxic and IR lung injury.[31,32] Although much work has been done in cell cultures and tissue homogenates, studies for probing key tissue mitochondrial functions and the effect of oxidant injury in the intact lungs are limited.[25] Thus, the objective of this study is to utilize cryoimaging to evaluate the effects of *in vivo* exposure of rats to hyperoxia or lung IR on lung tissue mitochondrial redox ratio (NADH/FAD). The results of this study will provide a basis to apply optical fluorescent techniques for evaluating the effects of these and other models of lung injury on lung tissue mitochondrial RR *in vivo*.

2 Materials and Methods

2.1 Hyperoxic Exposure

All animal experiments were performed under the approval of Institutional Animal Care and Use Committee review boards and in compliance with the National Research Council's Guide for the Care and Use of Laboratory Animals. Sprague-Dawley rats (275 to 350 g, males) were housed in a Plexiglas chamber maintained at 85% O_2 balance N_2 for 7 days as previously described.[33] Age-matched control rats were exposed to room air (21% O_2) and referred to as normoxic rats. This O_2 level and exposure period were chosen for several reasons. First, Crapo et al. provide detailed description of histologic and morphometric changes in lungs of rats exposed to this injury model.[26] Second, we have demonstrated that rat exposure to this hyperoxia model alters the activities of lung tissue mitochondrial complexes I, III, and IV.[33] Third, the rats are unique in that if preexposed to 85% O_2 for seven days, they develop tolerance to the otherwise lethal effects of exposure to 100% O_2.[26,33] Lungs were isolated immediately following the seven day exposure to controlled environmental gases as described under Sec. 2.3.

2.2 IR Injury

Adult Sprague-Dawley rats (∼300 g) were anesthetized with isoflurane, an endotracheal (ET) tube was secured for ventilation, and the rat placed in a prone position as previously described.[31] The left anterior chest was opened to access the left hilum. The left hilum, including the main stem bronchus, left pulmonary artery (PA), and left pulmonary veins, was located and clamped for 60 min, after which time the vascular clamp was removed and the surgical wound closed. Lungs for

imaging studies were harvested 24 h later, following the procedure for isolated perfused studies described under Sec. 2.3.

2.3 Isolated Lung Perfusion and KCN Administration

The isolated perfused and ventilated lung preparation has been previously described.[34] Briefly, each rat was anesthetized with pentobarbital sodium (40 mg/kg body wt i.p.), after which the chest was opened. Heparin (0.7 IU/g body wt) was injected into the right ventricle. Cannulas were placed in the pulmonary artery and the trachea, and the pulmonary venous outflow was accessed via a cannula in the left atrium. The lungs were removed from the chest and attached to a ventilation and perfusion system. The perfusate was Krebs-Ringer bicarbonate solution containing 3% bovine serum albumin. The ventilation gas mixture was 15% O_2, 6% CO_2 in N_2. The perfusate was pumped (at 10 ml/min) through the lung until it was clear of blood, after which the flow and ventilation were stopped. The lung was then partially deflated by disconnecting the tracheal cannula from the ventilation system then rapidly frozen as described below. The ventilation with room air ($PO_2 \sim 115$ mmHg) lasted for ∼15 min, and should have no effect on the mitochondrial redox state since the PO_2 at which mitochondrial complex IV activity is decreased and the electron transport chain reduced is <2 mmHg.[16] To determine the ability of the cryoimaging technique to detect a change in mitochondrial NADH and FAD redox state, for one group of normoxic rats the lungs were perfused with a solution containing potassium cyanide (KCN, complex IV inhibitor, 2 mM) for 5 min prior to freezing. This treatment was employed to reduce the respiratory chain, and hence increase NADH signal, decrease FAD signal, and as a result increase RR.

2.4 Freezing Protocol and Embedding

Lung tissue metabolic state was preserved by rapid freezing in chilled isopentane (2-methyl butane, Fisher Scientific, IL) within liquid nitrogen (LN_2, −196°C). The tissue was immersed in isopentane for 1 min followed by permanent storage in LN_2. For fluorescence imaging, the tissue was embedded in a customized black mounting medium (that is not fluorescent in the excitation wavelengths) and placed on a chilled aluminum plate to keep the tissue in place for freezing and slicing.

The mounting medium is prepared in the biophotonics lab (UWM), using polyvinyl alcohol (PVA, Grade 71-30, PVOH7130, Chemical Store Inc., Clifton, NJ), distilled water and carbon black powder (Daniel Smith Dry Pigment, 284030040, Daniel Smith, Inc., Seattle, WA). To make one liter of the embedding medium, 80 g of PVA is added to 920 g of boiling distilled water and stirred to make a homogeneous transparent medium. Then the solution is cooled down and 80 g of carbon black is added and mixed thoroughly and refrigerated for four to five days before use.

The embedding process starts with freezing the base medium, embedding the tissue and fixing its position by adding more black medium around the tissue. After embedding, the tissue was stored in an ultralow freezer (−80°C) for at least 24 h prior to imaging. The lungs were imaged within a week, with each injured group imaged along with its corresponding control group. The plate was then installed in the cryoimager where the surface of the black medium is parallel to a microtome.

2.5 Cryoimager

Low-temperature fluorescence imaging (cryoimaging) provides three-dimensional (3-D) fluorescence images of cryopreserved intact organs, and a higher quantum yield of fluorescence of NADH and FAD as compared to room temperature.[24,35,36] The cryoimager (Fig. 1) collects 3-D fluorescence images of frozen tissue's intrinsic or extrinsic fluorophores. The instrument consists of an Aqua Exi charge-coupled device (CCD) camera (Q-imaging, Aqua Exi, 14 bit, 6.45 μm pixel), a workstation (Dell computer), a mercury arc lamp (200 W, Oriel), an excitation (EX) filter wheel (which provides up to five excitation wavelengths), an emission (EM) filter wheel with synchronized rotation to EX wheel, and a cryostatic microtome. Fluorescence images are acquired with the digital camera (1392 × 1040 pixel array) with a 200 mm Nikkor lens (Nikon, Tokyo, Japan). Two motorized filter wheels containing excitation and emission filters are mounted in front of the light source and camera, respectively. The motor-driven microtome sequentially sections frozen tissue at the desired slice thickness while filtered light from the arc lamp excites fluorophores in the exposed surface of the tissue block for up to five distinct fluorophores. The microtome is housed in a freezer unit that maintains the sample at −40°C during sample slicing and image acquisition. Computer control of the microtome motor and filter wheels as well as image capture and display is accomplished through LabVIEW (8.6 National Instruments).[37]

The excitation band pass filter used for NADH is 350 nm (80 nm bandwidth, UV Pass Blacklite, HD Dichroic, Los Angeles, CA) and for FAD is 437 nm (20 nm bandwidth, 440QV21, Omega Optical, Brattleboro, VT). The emission filter for NADH is 460 nm (50 nm bandwidth, D460/50M, Chroma, Bellows Falls, VT) and for FAD is 537 nm (50 nm bandwidth, QMAX EM 510-560, Omega Optical, Brattleboro, VT). At each slice, the camera records fluorescence images of the tissue block in pixel dimensions of 22 × 22 μm. The resolution in the z direction of microtome slices can be as small as 10 μm. For this study, a resolution of 25 μm was used in the z direction, which resulted in ∼1000 z-slices per lung. Images are acquired with exposure times of 1.5 sec for FAD and 1 sec for NADH. Accounting for the time to rotate the filter wheels, as well as moving and slicing
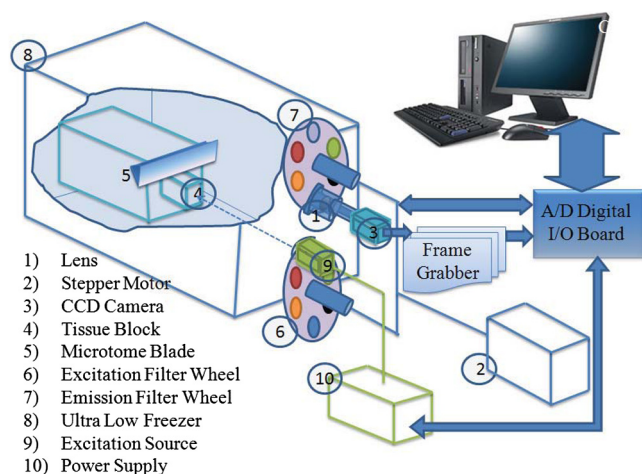
the sample, results in 3 to 4 h (depending on the size of the lung) for imaging the whole rat lung.

2.6 Calibration

A calibration method was designed to compensate for day-to-day variation of light intensity, mirror angle, and nonuniformity of the illumination pattern. At the beginning of each experiment and before slicing the tissue, a piece of graph paper was placed in the tissue position to set the focus of the lens and determine the resolution. Then, one image is taken with the lamp shutter closed and the camera lens covered, referred to as the dark image. Then a uniform fluorescent flat acrylic plate was placed in the same position and imaged in all channels to acquire the illumination pattern. Because of the fluorescence of the standard in both the NADH and FAD channels and its high resistance to photobleaching, it also accounts for day-to-day light intensity changes in all channels. The acrylic plate is also advantageous in that it allows for imaging with camera settings in the same range as those used for tissue without causing saturation of the resulting image. Acquisition of the tissue sections then proceeds.

When the tissue has been completely imaged, each individual slice first has the dark image subtracted from it, followed by correction for the nonuniformity of the illumination pattern by division of each image to the image of the flat plate captured in the same channel.

2.7 Image Processing

FAD and NADH autofluorescence images (containing 1000 slices per lung) from each of the four groups of lungs were processed using MATLAB (The MathWorks, Inc., Natick, MA). The composite images were created using all the image slices for each lung, for both NADH and FAD signals. The ratio of NADH and FAD, known as the mitochondrial redox ratio,[22,38] was calculated voxel by voxel, using Matlab, according to Eq. (1).

$$\text{Redox ratio} = \text{RR} = \text{NADH/FAD}. \tag{1}$$

For each lung, a histogram of RR values was created, and the mean (or first moment) of this histogram was calculated for the whole volume of the tissue according to Eq. (2).

$$\text{Mean} = \frac{1}{N_x \times N_y \times N_z} \sum_{i=1}^{N_x} \sum_{j=1}^{N_y} \sum_{k=1}^{N_z} \text{Lung\_Volume}(i, j, k), \tag{2}$$

where N_x, N_y, and N_z are the number of voxels in x, y, and z directions, respectively and the voxel size in x, y, and z direction is 22, 22, and 25 μm, respectively. Only the tissue volume was included in the calculation of the mean value and the background (from black medium) is excluded.

For the IR lungs, the left and right lobes were separated to examine similarities and differences between the injury region and the normal region. This was performed by defining a plane that separates the two lobes (using the voxels' inherent coordinate geometry), and collecting data on either side of the plane separately.
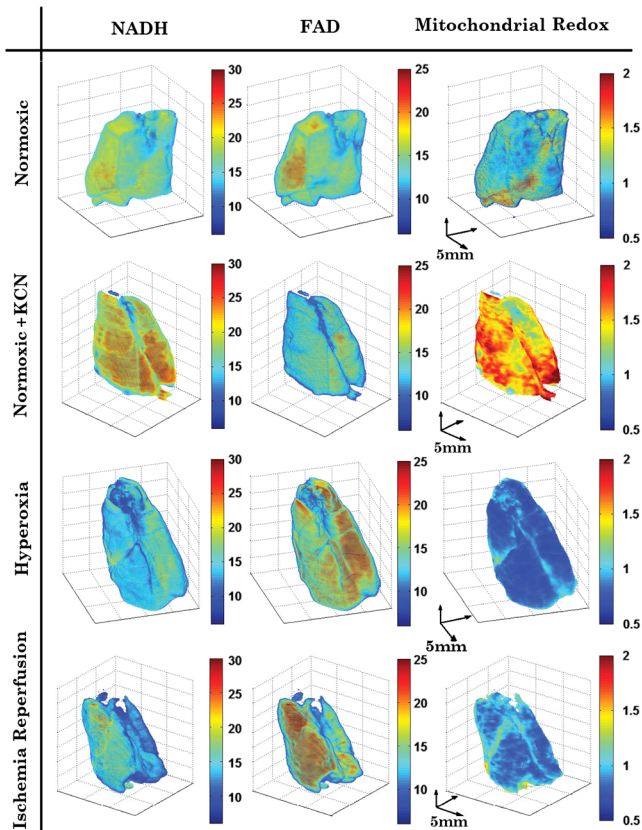

Fig. 1 Schematic of Cryoimager. This device sequentially slices the tissue, imaging the surface between each successive slice, in as many as five channels. The images are then displayed and saved to a computer, where they can be processed to create 3-D renderings of the tissue.[33]

1) Lens
2) Stepper Motor
3) CCD Camera
4) Tissue Block
5) Microtome Blade
6) Excitation Filter Wheel
7) Emission Filter Wheel
8) Ultra Low Freezer
9) Excitation Source
10) Power Supply

Fig. 2 Representative 3-D reconstructions of lungs from each of four groups (normoxic, normoxic + KCN, hyperoxic, and IR). From left to right, images shown are NADH, FAD, and mitochondrial redox ratio (RR).

2.8 Statistical Evaluation of Data

Statistical comparisons were carried out on a population of $N = 4$ in each group using a one-tailed student's t-test or one way ANOVA followed by Tukey's honestly significant difference (HSD) test, with $P < 0.05$ as the criterion for statistical significance.

3 Results

Figure 2 shows the 3-D rendering of NADH and FAD fluorescence signals and their ratio (RR = NADH/FAD) from representative lungs of each of the four groups (normoxic, normoxic + KCN, hyperoxic, and IR). As expected, lung treatment with KCN, which inhibits complex IV and hence reduces the chain, increased the NADH signal and decreased the FAD signal and as a result increased RR.

Figure 3 shows histograms of RR for the four sets of lungs in Fig. 2. For the IR lung, the histogram in Fig. 3 is that of both the injured lobe (left lobe) and normal lobe like the other sets. Despite the localized nature of the IR insult, all areas of the lung show a difference when compared to a normal lung. For each histogram, the mean value was calculated as described in Sec. 2. In Fig. 3, the counts of each bin have been normalized to the total number of pixels in the lung. As a result of this normalization, the value of each bin corresponds to the percent of voxels in the lung with intensities falling within the given range. In this manner, the histogram can be thought of as a scaled probability density function of mitochondrial redox ratio intensities for a lung. The mean values of these histograms suggest a more reduced mitochondrial redox state for normoxic lungs treated with KCN, and more oxidized mitochondrial redox state for hyperoxic and IR lungs as compared to normoxic lungs.

Figure 4 shows the average $\pm$ SE (standard deviation over the number of samples) of the mean values of the redox ratio histograms for all four groups of rats. Each lung was calibrated to correct for day-to-day variations as described in Sec. 2. In this figure, only the injured lobe of the lung was considered when generating the histograms of the IR lungs. Inhibition of complex IV with KCN increased the mean value of the RR histogram by 30% compared to normoxic lungs. On the other hand, hyperoxia and IR decreased the mean values of the RR histograms by 23% and 28%, respectively, compared to normoxic lungs.

Figure 5 displays a bar graph plot comparing the contralateral (nonischemic) lobe to the injured lobe of lungs subjected to ischemia-reperfusion. The figure shows that both NADH and FAD signals were decreased for the injured lobe as compared to the nonischemic lobe. However, the mitochondrial redox ratio was only minimally impacted.
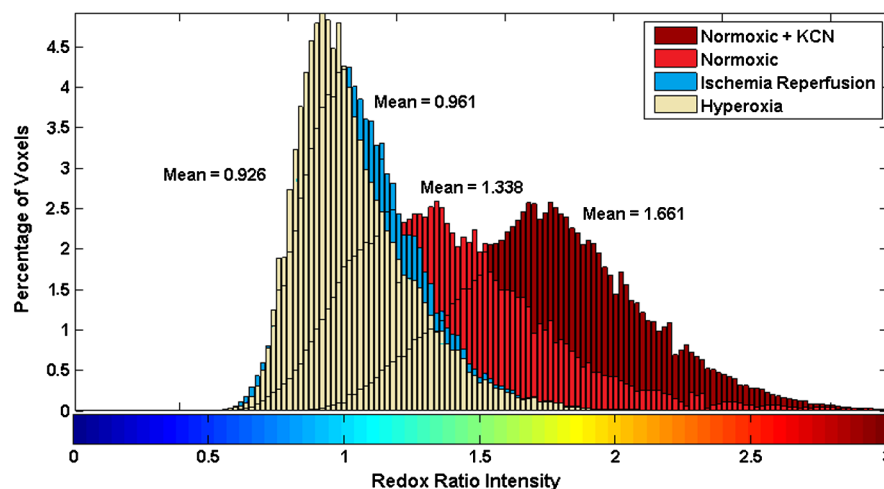

Fig. 3 Histogram distribution of Redox ratio for the four lungs displayed in Fig. 2.
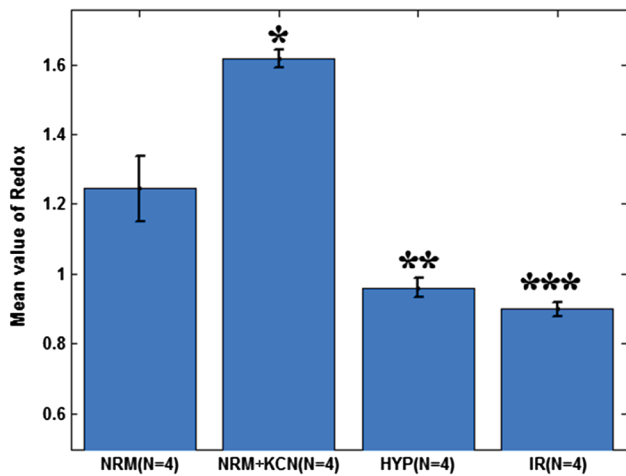
Fig. 4 Bar graph showing the average values and standard errors of the mean value of the histogram of the mitochondrial redox ratio for each of the four groups of lungs. The results show a difference between normoxic (NRM) and NRM + KCN (*$p < 0.005$), NRM and hyperoxic (HYP) (**$p < 0.01$), and NRM and IR (***$p < 0.005$). p values were obtained from post-hoc testing of a balanced one-way ANOVA using Tukey's honestly significant difference criterion.
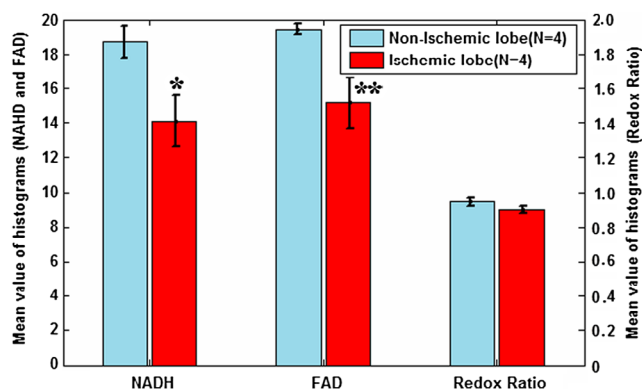

Fig. 5 Bar graph plot comparing the average values and standard errors of the mean value of the normal lobe to the IR lobe in IR lungs. The results show a difference between nonischemic (contralateral) and injured ischemic lobe in NADH (*$p < 0.01$) and FAD (**$p < 0.05$). p values were obtained from a paired one-tailed student's t-test.

4 Discussion and Conclusion

The results of this study demonstrate the utility of cryoimaging for evaluating the redox status of tissue mitochondrial coenzymes NADH and FAD in intact lungs. The redox ratio (RR), NADH/FAD, is an index of lung tissue mitochondrial redox state, which is an important determinant of mitochondrial bioenergetics.

The results revealed that both chronic hyperoxia and IR injury decreased lung RR due to mitochondrial dysfunction caused by oxidative stress. Although these two injury models produce the same mitochondrial dysfunction and caused oxidative stress, it is possible that they might be distinguished due to the heterogeneity of the IR injury. However, the present goal of this study is to quantify oxidative lung injury regardless of cause.

Previously, we demonstrated that rat exposure to 85% O_2 for seven days decreased complex I activity by 50% and increased complex III and IV activities by 56% and 90%, respectively, as

compared to normoxic lungs.[33] These changes would be expected to lead to a more oxidized chain downstream from complex I and hence could account for the decreased RR measured in this study.

Prediction of hyperoxia-induced lung injury is difficult because the susceptibility of individuals to hyperoxia is quite variable. Serial surface fluorescence measurements that can be obtained from catheter probes inserted through tube thoracostomies could provide critical real-time information regarding the development of oxidative lung injury over days in patients at risk.

The IR model also causes a depression in complex I activity, which would also be expected to oxidize the chain downstream from complex I and hence could account for the decrease in RR.[22] Our results show that RR decreased equally for both the ischemic and nonischemic lungs. This suggests that the IR injury was not limited to the ischemic lung. This is consistent with our previous results, which demonstrated an increase in caspase 3 activity and influx of neutrophils in *both* lungs in this IR model,[31] clearly demonstrating bilateral injury. The anesthesia "preconditioning" effects on the IR lungs tissue caused by isoflurane are minimized after a 24-h recovery period following the surgery. The left (ischemic and reperfused) and right (nonischemic) lungs would exhibit identical preconditioning effects if there are any.

Because IR is associated with alveolar hemorrhage[31,32] and *in vivo* estimates of RR would unavoidably be acquired in the presence of blood, we determined the effect of blood on RR as follows. We conducted cryoimaging for one control lung that was not washed free of blood and compared its NADH, FAD, and RR to those of control lungs that were washed of blood. Figure 6 demonstrates the effect of having blood present in the tissue, as would be the case for any *in vivo* study. The overall fluorescence signal decreased in both channels; however, the RR change is relatively small. This result is consistent with the results from a study by Chance et al. in which they showed that perfusion of isolated organs (e.g., liver) with perfusate containing red blood cells decreases NADH and FAD signals but does not change the redox ratio.[21] They concluded that the RR in the presence of blood is still a faithful indicator of
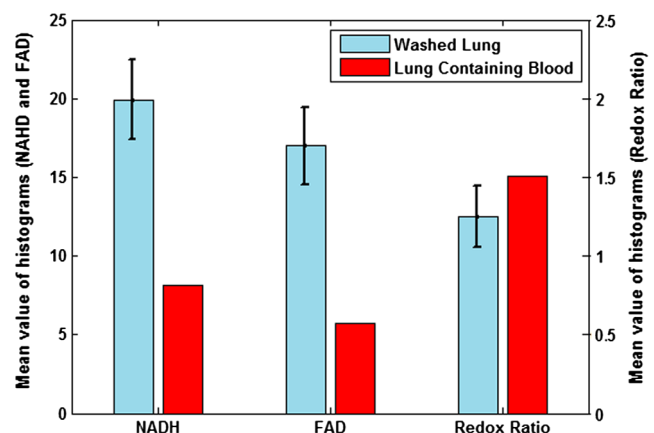

Fig. 6 Mean values of NADH, FAD, and RR histograms of two groups of normoxic lungs plus the standard deviation of the mean value for the first group. For the first group (washed lungs) the blood was washed out of the lungs ($n = 4$) by perfusing with Krebs bicarbonate solution. For the second (lung containing blood), the lung ($n = 1$) was not perfused and was frozen immediately after it was removed from the chest.

oxidation-reduction and can compensate for interfering factors such as light scattering and hemoglobin that exist under in vivo conditions.[21] Several methods exist to correct for these factors, with the most commonly used technique involving normalizing the fluorescence to a reflectance measurement taken at each excitation wavelength.[39,40]

Cytosolic NADPH, which has the same fluorescence characteristics as NADH, could be contributing to the signal attributed to NADH in this study. However, Chance et al. demonstrated that the fluorescence signal originates mostly from NADH in the mitochondria and the contribution of NADPH—present in cytosol—is very small.[41] This is consistent with the fact that the quantum yield for NADH is much higher than NADPH (2.5 to 1.25), and its concentration is five times larger than NADPH.[42–44] Thus, NAPDH contribution to the NADH signal and the change in the NADH signal due to hyperoxia or IR in this study is assumed to be small.

Other endogenous fluorophores that may contribute to the NADH signal include collagen and elastin, which are present in the tissue.[45] However unlike NADH, collagen and elastin contribution would not be expected to change with variations in mitochondrial redox state.[45,46]

The current study demonstrates the utility of RR to detect lung mitochondrial oxidant injury under ideal conditions that optimize the quantum yields of NADH and FAD and minimize the effects of confounding factors such as blood. We have not evaluated the effect of temperature on the quantum yields of NADH and FAD. However, Chance et al. addressed this question and demonstrated a high correlation between the RR values in room temperature compared to cryogenic temperatures.[21] In addition, we have developed a fluorometer to measure lung-surface NADH and FAD signals from an isolated perfused lung at 37°C. Preliminary results using this system in an isolated perfused rat lung revealed that lung treatment with the complex IV inhibitor potassium cyanide (KCN) increased the NADH signal and decreased the FAD signal, and as a result increased the RR in close correlation with that observed in cryoimaging results (Fig. 4). This suggests that the RR is less sensitive to temperature than the quantum yields of NADH and FAD.

The results of this study support the utility of optical imaging of NADH and FAD signals to evaluate lung tissue mitochondrial redox state. While optical determination of RR in tissues such as brain and myocardium is accepted,[19,20,39] the applicability of these methodologies in examination of the redox state in lungs, where the density of mitochondria is much lower, has not been established. The potential clinical importance of real-time optical imaging of lungs in patients with critical illness, patients on high O_2, or patients with IR lung injury secondary to lung transplant, chest contusions, is great. Reliable fluorescence determination of RR could be adopted in the same fashion that near-infrared spectroscopy (NIRS) is gaining favor as a non-invasive measure of tissue oxygenation in critically injured patients.[47] While NIRS is an indirect measure of tissue oxygenation, NADH and FAD data provide information regarding tissue redox and mitochondrial bioenergetics, a truer and more sensitive early measure of organ function. Because NADH and FAD signals can be detected through fiber optic probes placed on the surface of the lung, RR data could be obtained either intraoperatively or through tube thoracostomies (frequently placed for clinical indications in patients with severe lung injury). Our studies support the capacity of fluorescence imaging to detect pulmonary oxidative injury, and set the stage for *in vivo* studies along with adaptation of the methods (use of reflectance measurements) required to translate this approach to clinical arenas.

References

1. T. Vo-Dinh, *Biomedical Photonics Handbook*, CRC Press, USA (2000).
2. C. H. Barlow et al., "Fluorescence mapping of mitochondrial redox changes in heart and brain," *Crit. Care Med.* **7**(9), 402–406 (1979).
3. E. Meirovithz, J. Sonn, and A. Mayevsky, "Effect of hyperbaric oxygenation on brain hemodynamics, hemoglobin oxygenation and mitochondrial NADH," *Brain Res. Rev.* **54**(2), 294–304 (2007).
4. A. P. Michalopoulou et al., "Spectroscopic imaging for detection of ischemic injury in rat kidneys by use of changes in intrinsic optical properties," *Appl. Opt.* **44**(11), 2024–2032 (2005).
5. R. S. Balaban and L. J. Mandel, "Coupling of aerobic metabolism to active ion transport in the kidney," *J. Physiol.* **304**, 331–348 (1980).
6. S. Maleki et al., "Mitochondrial redox studies of oxidative stress in kidneys from diabetic mice," *Biomed. Opt. Express* **3**(2), 273–281 (2012).
7. B. Vollmar et al., "A correlation of intravital microscopically assessed NADH fluorescence, tissue oxygenation, and organ function during shock and resuscitation of the rat liver," *Adv. Exp. Med. Biol.* **454**, 95–101 (1998).
8. S. Nioka et al., "Simulation of Mb/Hb in NIRS and oxygen gradient in the human and canine skeletal muscles using H-NMR and NIRS," *Adv. Exp. Med. Biol.* **578**, 223–228 (2006).
9. N. Ramanujam et al., "In vivo diagnosis of cervical intraepithelial neoplasia using 337 nm-excited laser-induced fluorescence," *Proc. Natl. Acad. Sci. USA* **91**(21), 10193–10197 (1994).
10. M. A. Mycek, K. T. Schomacker, and N. S. Nishioka, "Colonic polyp differentiation using time-resolved autofluorescence spectroscopy," *Gastrointest. Endosc.* **48**(4), 390–394 (1998).
11. N. Ramanujam et al., "Fast and noninvasive fluorescence imaging of biological tissues in vivo using a flying-spot scanner," *IEEE Trans. Biomed. Eng.* **48**(9), 1034–1041 (2001).
12. G. A. Wagnieres, B. C. Wilson, and W. M. Star, "In vivo fluorescence spectroscopy and imaging for oncological applications," *Photochem. Photobiol.* **68**(5), 603–632 (1998).
13. N. Ramanujam et al., "Low temperature fluorescence imaging of freeze-trapped human cervical tissues," *Opt. Express* **8**(6), 335–343 (2001).
14. B. Chance and G. R. Williams, "A method for the localization of sites for oxidative phosphorylation," *Nature* **176**(4475), 250–254 (1955).
15. A. Mayevsky, "Brain NADH redox state monitored *in vivo* by fiber optic surface fluorometry," *Brain Res.* **319**(1), 49–68 (1984).
16. A. B. Fisher, "Intermediary metabolism of the lung," *Environ. Health Perspect.* **55**, 149–158 (1984).
17. B. Chance and H. Baltscheffsky, "Respiratory enzymes in oxidative phosphorylation, VII. binding of intramitochondrial reduced pyridine nucleotide," *J. Biol. Chem.* **233**(3), 736–739 (1958).
18. M. Ranji et al., "Fluorescence spectroscopy and imaging of myocardial apoptosis," *J. Biomed. Opt.* **11**(6), 064036 (2006).
19. M. Matsubara et al., "*In vivo* fluorometric assessment of cyclosporine on mitochondrial function during myocardial ischemia and reperfusion," *Ann. Thorac. Surg.* **89**(5), 1532–1537 (2010).
20. M. Ranji et al., "Quantifying acute myocardial injury using ratiometric fluorometry," *IEEE Trans. Biomed. Eng.* **56**(5), 1556–1563 (2009).
21. B. Chance et al., "Oxidation-reduction ratio studies of mitochondria in freeze-trapped samples. NADH and flavoprotein fluorescence signals," *J. Biol. Chem.* **254**(11), 4764–4771 (1979).

22. B. Chance, C. P. Lee, and B. Schoener, "High and low energy states of cytochromes, II. in submitochondrial particles," *J. Biol. Chem.* **241**(20), 4574–4576 (1966).
23. A. Shiino et al., "Three-dimensional redox image of the normal gerbil brain," *Neuroscience* **91**(4), 1581–1585 (1999).
24. B. Quistorff, J. C. Haselgrove, and B. Chance, "High spatial resolution readout of 3-D metabolic organ structure: an automated, low-temperature redox ratio-scanning instrument," *Anal. Biochem.* **148**(2), 389–400 (1985).
25. A. B. Fisher, L. Furia, and B. Chance, "Evaluation of redox state of isolated perfused rat lung," *Am. J. Physiol.* **230**(5), 1198–1204 (1976).
26. J. D. Crapo et al., "Structural and biochemical changes in rat lungs occurring during exposures to lethal and adaptive doses of oxygen," *Am. Rev. Respir. Dis.* **122**(1), 123–143 (1980).
27. W. A. Altemeier and S. E. Sinclair, "Hyperoxia in the intensive care unit: why more is not always better," *Curr. Opin. Crit. Care* **13**(1), 73–78 (2007).
28. A. B. Fisher and M. F. Beers, "Hyperoxia and acute lung injury," *Am. J. Physiol. Lung Cell Mol. Physiol.* **295**(6), L1066; author reply L1067 (2008).
29. C. S. Ng, S. Wan, and A. P. Yim, "Pulmonary ischaemia-reperfusion injury: role of apoptosis," *Eur. Respir. J.* **25**(2), 356–363 (2005).
30. http://www.infoplease.com/science/health/us-transplants-year.
31. I. Ali et al., "Protection by 20-5,14-HEDGE against surgically-induced ischemia reperfusion lung injury in rats," *Ann. Thorac. Surg.* **93**(1), 282–288 (2012).
32. A. Leke-Tambo et al., "The role of TLR4 and HMGB1 in the ischemia/reperfusion-mediated mitochondrial dysfunction," *Chest* **140**(4) (2011).
33. Z. Gan et al., "Differential responses of targeted lung redox enzymes to rat exposure to 60 or 85% oxygen," *J. Appl. Physiol.* **111**(1), 95–107 (2011).
34. S. H. Audi et al., "Coenzyme Q1 redox metabolism during passage through the rat pulmonary circulation and the effect of hyperoxia," *J. Appl. Physiol.* **105**(4), 1114–1126 (2008).
35. A. Mayevsky and B. Chance, "Oxidation-reduction states of NADH in vivo: from animals to clinical use," *Mitochondrion* **7**(5), 330–339 (2007).
36. J. J. Kelly et al., "Regional blood flow measurements from fluorescent microsphere images using an Imaging CryoMicrotome," *Rev. Sci. Instrum.* **71**(1), 228–234 (2000).
37. S. L. Bernard et al., "High spatial resolution measurements of organ blood flow in small laboratory animals," *Am. J. Physiol. Heart Circ. Physiol.* **279**(5), H2043–H2052 (2000).
38. B. Chance and H. Baltscheffsky, "Respiratory enzymes in oxidative phosphorylation, VII. binding of intramitochondrial reduced pyridine nucleotide," *J. Biol. Chem.* **233**(3), 736–739 (1958).
39. A. Mayevsky and G. G. Rogatsky, "Mitochondrial function in vivo evaluated by NADH fluorescence: from animal models to human studies," *Am. J. Physiol. Cell Physiol.* **292**(2), C615–C640 (2007).
40. A. Mayevsky et al., "Mitochondrial function and tissue vitality: bench-to-bedside real-time optical monitoring system," *J. Biomed. Opt.* **16**(6), 067004 (2011).
41. B. Chance et al., "Intracellular oxidation-reduction states in vivo," *Science* **137**(3529), 499–508 (1962).
42. L. K. Klaidman, A. C. Leung, and J. D. Adams Jr., "High-performance liquid chromatography analysis of oxidized and reduced pyridine dinucleotides in specific brain regions," *Anal. Biochem.* **228**(2), 312–317 (1995).
43. M. O'Connor et al., "Origin of labile NADH tissue fluorescence," *Oxygen Physiol. Funct.* **10**, 10, 1977.
44. Y. Avi-Dor et al., "Fluorescence of pyridine nucleotides in mitochondria," *Biol. Chem.* **237**(7), 7 (1962).
45. I. Georgakoudi et al., "NAD(P)H and collagen as in vivo quantitative fluorescent biomarkers of epithelial precancerous changes," *Cancer Res.* **62**(3), 682–687 (2002).
46. N. Ramanujam et al., "In-vivo diagnosis of cervical intraepithelial neoplasia using 337 nm-excited laser-induced fluorescence," *Proc. Natl. Acad. Sci. USA* **91**(21), 10193–10197 (1994).
47. N. I. Shapiro et al., "The association of near-infrared spectroscopy derived tissue oxygenation measurements with sepsis syndromes, organ dysfunction, and mortality in emergency department patients with sepsis," *Crit. Care* **15**(5), R223 (2011).